Bulletin of Environmental Contamination and Toxicology (2019) 103:267–273
https://doi.org/10.1007/s00128-019-02642-w

A Near-infrared Persistent Luminescence Imaging Technique for Tracking Nanoparticles in Zebrafish (*Danio rerio*)

Chengcheng Wang[1,2] · Shenghui Zheng[1,2] · Xiaoyan Zou[1] · Xia Sun[1] · Hongwu Zhang[1]

Received: 29 November 2018 / Accepted: 31 May 2019 / Published online: 6 June 2019

Abstract

The development of nanotechnology has drawn increased attention to the risks of nanoparticles (NPs). In this work, the near-infrared persistent luminescence imaging technique was used to track the biodistribution of NPs in vivo in zebrafish. Zebrafish were used as a vertebrate animal model to show NPs distribution and the effects of exposure. $ZnGa_2O_4$:Cr (ZGOC) was chosen as the probe in this work. In continuous exposure experiments, the results showed more particles accumulated in the intestines than in the gills in both groups. In both the gills and abdomen, the NPs contents were greater in the ZGOC–NH_2-treated groups than in the ZGOC groups, and the NPs caused damage to the gills and intestines. Removal exposure experiments indicated that ZGOC and ZGOC–NH_2 could be excreted from the body. The metabolism, excretion of NPs, the quantification and monitoring of NPs behavior in biological systems should be examined in further studies.

Keywords Near-infrared persistent luminescence · Nanoparticles · In vivo imaging · Distribution · Zebrafish

Engineered nanoparticles (NPs) have increasingly entered the environment. The risks posed by these NPs to the environment and health have also increased (Furman et al. 2013). The substantial differences in physicochemical properties between nanomaterials and bulk-phase materials have been recognized in numerous scientific and technological areas (Mahmoudi et al. 2010). Nanomaterials can enter the body and might interact with intracellular structures and macromolecules over a long duration. With the rapid increase in nanomateial-based products, including NPs, NPs have been released into aquatic environment without further treatment (Wiesner et al. 2006), and have inevitably entered aquatic organisms, ultimately affecting higher organisms through food chains (Zhu et al. 2010). Due to their ability to pass through the blood–brain barrier and deposit in cells and tissues, NPs can affect and damage normal functions. NPs might also interfere with the cell surface structure, causing disorders in cell metabolism and inducing cell apoptosis or necrosis.

Therefore, there is a growing demand for detecting and monitoring nanomaterials to better understand the influence of NPs on organisms. However, in addition to NPs' small-size effect, conventional methods still have many limitations in tracking and displaying of NPs in animals. Electron microscopy methods display a partial but not a full view of organisms. ICP-MS detects NPs quantitatively, but it cannot discriminate between NPs and ions. Therefore, optical imaging techniques can address the disadvantages mentioned above as an ideal solution. With the development of in vivo optical imaging, this technique has become a powerful research tool in the field of biomedicine. As one type of in vivo imaging technology, persistent luminescence imaging has emerged recently (Chermont et al. 2007). Due to the minimal biological damage caused by this technique and repeatedly re-charged in situ external excitation, high signal-to-noise ratio in vivo images have been obtained, thus have attracting even more attention. However, this imaging technique still has some shortcomings. The surface of persistent luminescence NPs lacks active organic groups that can form interactions with biomolecules. Furthermore, controllable methods for the synthesis of monodisperse NPs with

Electronic supplementary material The online version of this article (https://doi.org/10.1007/s00128-019-02642-w) contains supplementary material, which is available to authorized users.

✉ Hongwu Zhang
hwzhang@iue.ac.cn

[1] Key Laboratory of Urban Pollutant Conversion, Institute of Urban Environment, Chinese Academy of Sciences, Xiamen 361021, China

[2] University of Chinese Academy of Sciences, Beijing 100049, China

high luminescent intensity and long persistent duration are still scarce. However, a sol–gel method was used to synthesize persistent luminescence materials, and suitable NPs were selected via separation and screening. After in vitro excitation, the NPs were injected into mice through the tail vein to realize real-time optical imaging of the living body for up to an hour, which addressed the above deficiencies. The emergence and development of persistent luminescence materials probes at the nanoscale (Zou et al. 2017a, b) have expanded their application domains. A new generation of persistent luminescence materials emitting in the near-infrared (NIR) range provides improved tissue penetrability and can be monitored in real time without excitation light or substrate injection. The NIR persistent luminescence imaging technique can spatially and quantitatively monitor nanoprobes in vivo to minimize cytotoxicity.

In addition to the advantages of low space requirements, low-cost maintenance, short generation cycle, and rapid development, zebrafish (*Danio rerio*) have been widely used as a model organism due to the similarity between their gene sequences and organ systems and those of humans (Love et al. 2004; Stern and Zon 2003). The zebrafish is also an ideal model organism for bioimaging due to its relative transparency.

Some studies have reported the distribution of probes, such as quantum dots, in animals (e.g. nematodes, mice). However, the use of persistent luminescence materials in zebrafish is rare. In this work, we used an NIR persistent luminescence imaging technique as an innovative in vivo method to detect and monitor the migration and distribution of NPs in zebrafish. To evaluate the effects of surface groups, two types of NPs with different surface groups were used in this study. This research was also conducted to explore the potential risks of the presence and application of NPs in water.

Materials and Methods

$Ga(NO_3)_3{\cdot}6H_2O$, $Zn(NO_3)_2{\cdot}6H_2O$ and $Cr(NO_3)_3{\cdot}9H_2O$ were obtained from Aladdin (Shanghai, China). Ammonia solution (28%), citric acid monohydrate, and absolute ethanol were purchased from Sinopharm Chemical Reagent (Shanghai, China). Tetraethyl *ortho*silicate (TEOS) (3-aminopropyl)-triethoxysilane (APTES), dimethylsulfoxide (DMSO) and methyl thiazolyl tetrazolium (MTT) were sourced from Sigma-Aldrich (USA). Human umbilical vein endothelial cells were obtained from the Cell Resource Center of the Shanghai Institutes for Biological Sciences (SIBS, China).

According to a previous study, ZGOC NPs were synthesized via a sol–gel method (Sun et al. 2018). Briefly, Zn^{2+}, Ga^{3+}, and Cr^{3+} were mixed in a molar ratio as $ZnGa_2O_4{:}Cr_{0.005}$. After addition of 2 g of citric acid, the above mixture was stirred to form a viscous gel in a drying oven. Then, the gel was sintered at 800 °C. According to previous reports (Li et al. 2014; Shi et al. 2015), NH_2 layers were obtained on the ZGOC NPs via surface modification. Briefly, ZGOC NPs were first hydroxylated by suspension in NaOH solution. Subsequently, hydroxyl-ZGOC particles were surface modification by APTES. Then, ZGOC–NH_2 NPs were obtained.

Transmission electron microscopy (TEM, Hitachi, Japan) was used to characterize the morphology of the samples and the mean size of the particles, and to view histological section at 100 kV. A PANalytical X' pert PRO diffractometer equipped with Cu Kα radiation (k = 1.5418 Å) was used to perform X-ray powder diffraction (XRD) analysis at room temperature. The zeta potentials were measured using a Malvern Zeta-sizer 3000 HS instrument. The electrophoretic mobility of the charged NPs was determined in an electric field at 25°C. Automatic measurements (10–100 runs) were performed in triplicate. An FLS920 spectrometer (Edinburgh, UK) was used to acquire excitation and emission spectra and determine the NIR afterglow decay. A Nicolet iS10 spectrometer (Thermo Scientific, USA) recorded the Fourier transform infrared spectroscopy (FTIR) spectra.

A cell viability assay (MTT) was conducted to measure the cytotoxicity of ZGOC and ZGOC–NH_2 NPs. The MTT assay was performed according to Sun et al. (2018).

Adult zebrafish were obtained from a market (Xiamen, China). Animal care and maintenance protocols were approved by the Animal Ethical Experimentation Committee of Xiamen University in accordance with the requirements of the National Act on the Use of Experimental Animals (China).

An IVIS Lumina II imaging system was used to demonstrate the distribution of NPs in zebrafish. Zebrafish were exposed to one of the following treatments: (1) continuous exposure to one of the two types of solution (ZGOC or ZGOC–NH_2) for 30 days or (2) exposure to one of the two types of solution for 10 days, followed by breeding in clean cultivation water. The zebrafish housing conditions are shown detailed in supplementary information (SI). The detailed process of bioimaging is also provided in the SI. The values are presented as the means ± standard deviations (SDs) in a triplicate experimental set. Variation analysis was conducted with one-way analysis of variance (ANOVA) at $p < 0.05$ via PAST. Histological sections were obtained with the protocol described in the SI.

Results and Discussion

TEM revealed that NPs had irregular morphologies (Fig. S1a, b), with diameters ranging from 30 to 100 nm. The XRD results (Fig. S1c) showed a typical spinel phase

of $ZnGa_2O_4$ (JCPDS Card No. 71–0843). ZGOC and ZGOC–NH_2 have similar excitation and emission spectra (Fig. S2a). After excitation at 254 nm, a narrow-band emission peak appeared at 696 nm. After irradiation with a white-light LED lamp for 5 min, the long-afterglow intensity was monitored at 698 nm, and the intensity slowly decayed with time. The persistent luminescence intensity was maintained for over 30 min (Fig. S2b). The surface modification of the NPs was confirmed by zeta potential analysis and FTIR spectra (Fig. S3). The surface zeta potentials of ZGOC and ZGOC–NH_2 were 4.79 and 21.6 mV, respectively (Fig. S3a). The change in zeta potential after the amination process supported the success of the amination modification. In addition, two strong absorption bands at 3423 cm^{-1} (N–H) and 1012 cm^{-1} (Si–O–R) appeared in the FTIR spectra, again indicating surface modification of the NPs with amines (Fig. S3b).

Nanoprobes with low toxicity are critical for in vivo or in vitro studies (Shi et al. 2015; Maldiney et al. 2014). After 24 h of incubation, the viability showed minimal obvious changes (Fig. S4). Following treatment with 100 mg/L ZGOC and ZGOC–NH_2, the cell viabilities were 95.1% and 95.3%, respectively. Therefore, the ZGOC and ZGOC–NH_2 NPs induced minimal cytotoxicity and were ideal probes for in vivo imaging. Although the behaviors of the zebrafish were normal at all experimental intervals, a limited number of zebrafish died during the experimental periods.

To confirm the lowest detectable dose, different volumes of ZGOC/ZGOC–NH_2 NP suspensions were injected into a pork sample (detailed in Fig. S5). Then, the linearity of the signals generated by varied amounts of NPs was obtained and is shown in Fig. S5. Figure 1 shows the process of continuous exposure: ZGOC/ZGOC–NH_2 NPs with different surface groups entered the fish. In the first two days, a substantial number of NPs were detected in the gills and abdomen of the two groups. In the gills, the signal intensities of ZGOC were much higher than those of ZGOC–NH_2 at the corresponding time point (D1, D3). The NPs the transferred from the gills to the abdomen. There was a significant difference on D1 between the two groups in the gills and abdomen. On D10, the NP signals in the gills decreased sharply, and NPs were mainly located in the abdomen. In the following days, the signal intensities in the gills of both groups were generally unchanged, whereas the NP contents in the abdomen increased with exposure time. After 30 days of exposure, the NPs were primarily accumulated in the

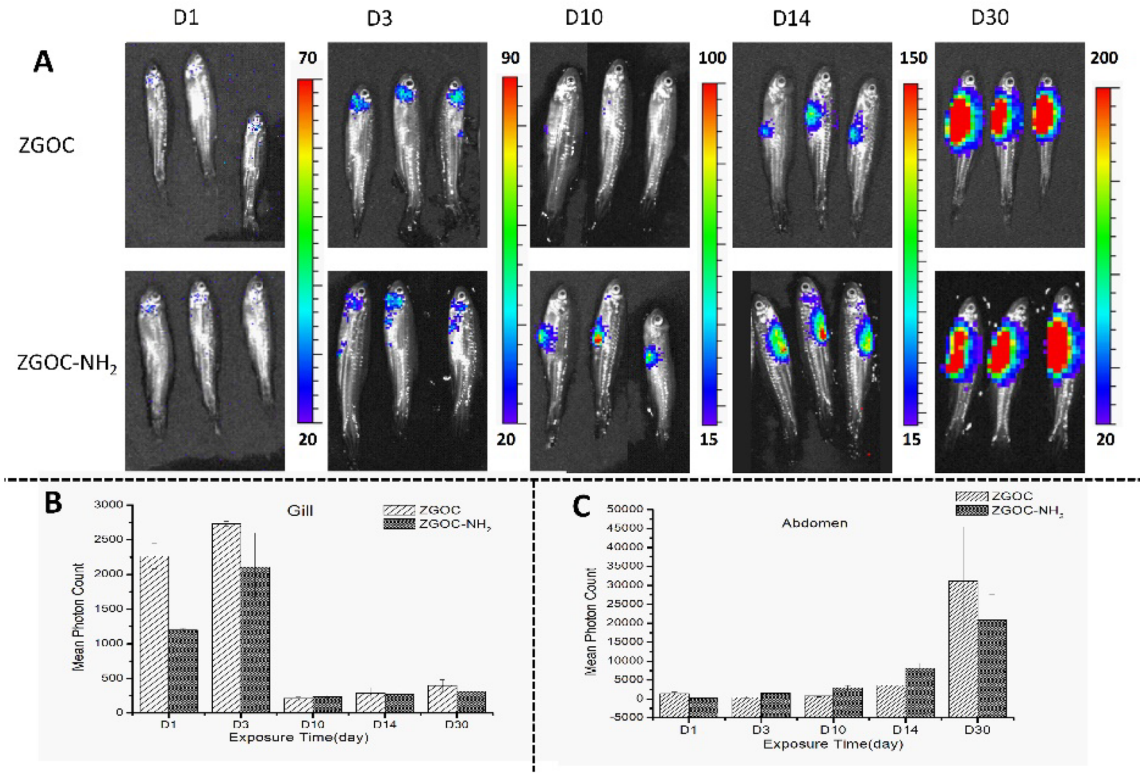

Fig. 1 Detection sensitivity for ZGOC/ZGOC–NH_2 in vivo. **a** In vivo luminescence images of zebrafish after 120 s of irradiation with a white-light LED lamp. The scale of luminescent intensity ranges from 20 to 70, 20 to 90, 15 to 100, 15 to 150, and 20 to 200. **b** and **c** The mean photon count of different parts of zebrafish in the two groups. Error bars represent the SD in a triplicate experimental set. "*" indicates significant differences between the two groups ($p < 0.05$)

abdomen. Moreover, few NPs were found in other organs. Although there were significant differences in the abdomen (D3, D10 and D14), different surface groups had little effect on the migration process of NPs in this work. The two NPs with the same positive zeta potential could be the reason for this. Previous studies indicated that gastrointestinal absorption often serves as the prevalent exposure route (Bergin and Witzmann 2013) and that the intestinal tract has absorptive functions. Absorption was a potential outcome of NP ingestion, which might explain why the NPs accumulated in the abdomen.

To investigate the distribution of the two NPs in organs after continuous exposure, we dissected the main viscera of the zebrafish and detected the signal strength on D14 and D30 (Figs. 2, S6). The signal intensities of the digestive tracts in both groups were significantly higher than those of other organs, which suggested the NPs mainly accumulate in the gastrointestinal tract. The results are consistent with the results mentioned above (Fig. 1) and the results from a previous study (Bisesi et al. 2014). Generally, toxic reactions such as hemolysis are more likely to be induced by cationic surface materials because of their affinity for negative phospholipid groups or proteins on cell membranes. Plasma protein binding can also be affected by surface charge. This phenomenon affects in vivo organ distribution and NP elimination from the circulation (Saxena et al. 2007).

The gills of both groups were damaged to different degrees, and certain organelles displayed swelling or cavitation phenomena (Fig. 3a, b) on D30. The suspended ZGOC/ZGOC–NH_2 NPs can adhere to the mucus in gills. Mucus secretion increased the epithelial cells in the cheeks. This process could lead to a lack of oxygen. Within a certain concentration range, the fish can remove the adherent particles via certain reactions. Therefore, a decrease in particle signal intensities was observed. It was found that acute and chronic exposure could induce a series of ultrastructural alterations in gill cells. Due to their functions of gas exchange, hydromineral control, acid–base balance and nitrogen excretion, the gills are crucial for maintaining homeostasis in fish (Leguen and Prunet 2004; Evans et al. 2005).

Figure 4 shows the differences between intestines treated with ZGOC and those treated with ZGOC–NH_2. The intestinal structure was in good condition (D1). Free surface epithelial cells were densely packed with neat microvilli (Fig. 4a–d). The columnar epithelium consisted of high cells joined through clear complete junctional complexes with intact and organized brush borders. On D30, hyperemia and mild edema were observed in the intestines after dissection, but no obvious change in the length and hardness of the intestines was noted. Enterocytes presented large light vacuoles in both groups. In the ZGOC-treated group, obvious morphological changes were noted in the intestinal epithelial cells. The microvilli became sparse and were no longer neatly arranged. This change was consistent with the results of Bisesi et al.'s research (2014). In the ZGOC–NH_2-treated group, the intestinal epithelial cells and microvilli were nearly unchanged. Interactions between intestinal cells

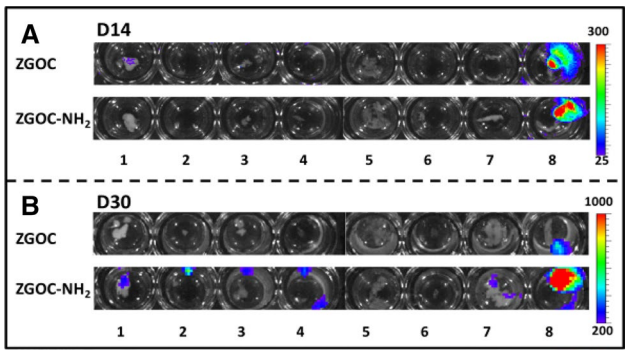

Fig. 2 In vitro luminescence images of zebrafish organs. **a** Luminescence images of isolated organs after continuous exposure to ZGOC/ZGOC–NH_2 for 10 days. The scale ranges from 25 to 300. **b** Luminescence of different organs after continuous exposure to ZGOC/ZGOC–NH_2 for 30 days. The scale ranges from 200 to 1000. (*1*) Brain (*2*) heart (*3*) liver (*4*) spleen (*5*) gill (*6*) kidney (*7*) gonads, and (*8*) gut

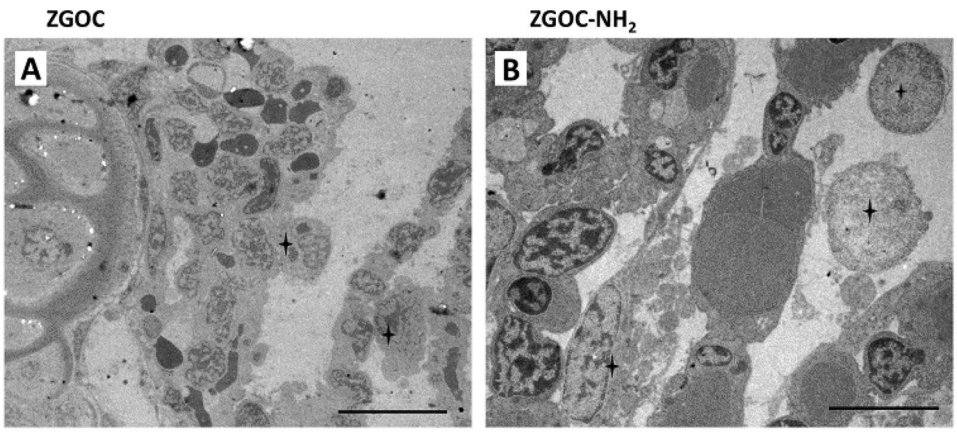

Fig. 3 TEM images of zebrafish gills exposed to ZGOC and ZGOC–NH_2 for 30 days. Bar **a** 10 μm and bar **b** 5 μm. The cells marked with a cross were hyperplastic/swollen

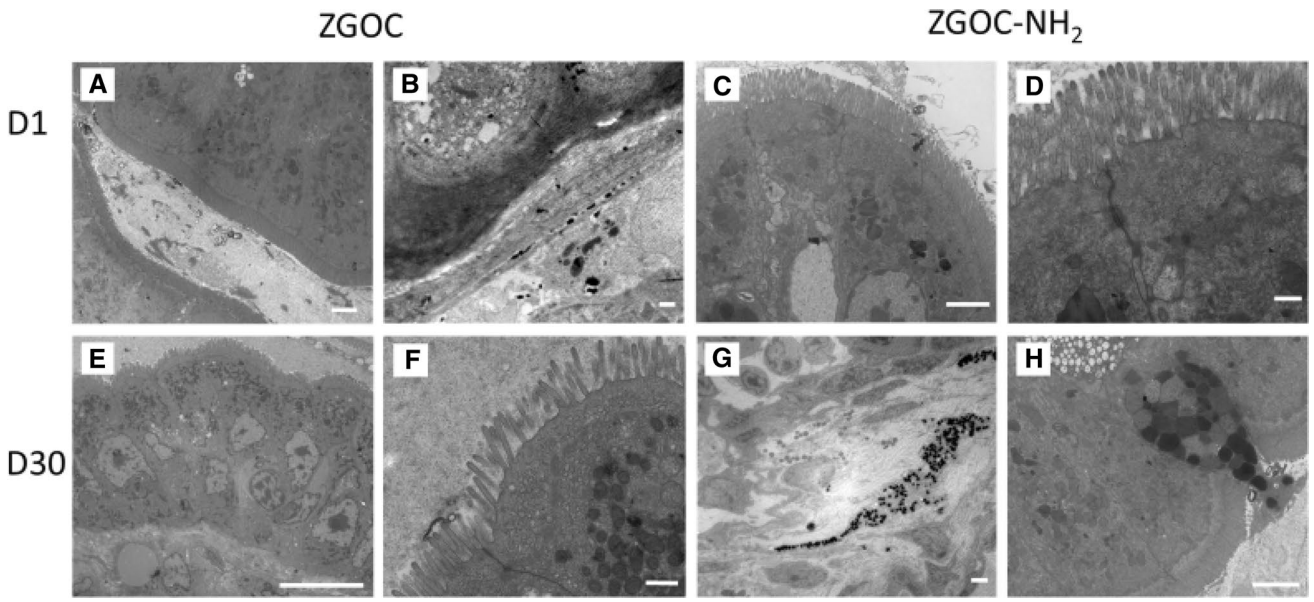

Fig. 4 TEM images of zebrafish intestines exposed to ZGOC and ZGOC–NH_2 for 1 and 30 days. **a**–**d** Images of the intestine after exposure for 1 day (marked as D1). **e**–**h** are images of the intestine after exposure for 30 days (marked as D30). **a**, **b**, **e** and **f** Images of groups treated with ZGOC. **c**, **d**, **g** and **h** Images of groups treated with ZGOC–NH_2. Bar **a**, **c**, **g** and **h** 2 μm, bar **b**, **d**, and **f** 0.5 μm and bar **e** 10 μm

and NPs, including deposition and/or effects on motility, could be a reasonable explanation for this result. The positive surface charge of the particles prevents adhesion and facilitates penetration. NPs adhered to mucin and aggregated NPs might disrupt the architecture of the mucus and gills, which enables penetration caused by subsequent exposure. Figure 4 also shows the fusion of pinocytosis vesicles and lysosomes. In other words, endocytosis was active, and NPs accumulated in this manner in the intestinal cells. This observation illustrated another explanation of why the accumulation of a large number of NPs can be detected in the digestive tract. In certain TEM images, we observed that mast cells released mucinogen granules within the lumen. Although this release can be spontaneous, it could also be caused by intestinal stimulation induced by the accumulation of NPs. Further studies are needed.

Although the in vitro MTT results indicated low cytotoxicity of ZGOC/ZGOC–NH_2, the in vivo results showed differences. NP toxicity in the body can be caused by different mechanisms, but the most likely reason for intracellular and in vivo toxicities from NPs is excess reactive oxygen species (Nel et al. 2006; Moller et al. 2010). Nel et al. noted that cell signaling might be affected by NP-induced oxidative stress in three stages (Rallo et al. 2011). Intensive research on this topic is necessary in future work.

The interaction between NPs and biosystem is rather intricate and dynamic in vivo. Due to the interactions with biological components, NPs can be absorbed after their entry into the body. Subsequently, the NPs could remain in the same structure or could be modified or metabolized after distribution into diverse organs (Borm et al. 2006). The period of time before NPs are transferred from the organs in which they enter the cells to another location or are excreted is unknown. However, we do know that NPs are found in feces (Deng et al. 2007; Yang et al. 2007).

To further evaluate NP metabolism, we conducted removal treatment. Figure 5 shows the process by which ZGOC/ZGOC–NH_2 NPs distributed in the body. The results for the gills (Fig. 5b) revealed differences between the two groups. When the NP administration was removed, the signals of the two groups increased on the first day (D11-). The signals of ZGOC reduced (D13-) and subsequently increased (D17-), whereas the signals of ZGOC–NH_2 NPs in gills decreased gradually. The abdominal results for both groups also show differences. On D11-, the signal intensity of the ZGOC–NH_2-treated group decreased, whereas that of the ZGOC-treated group increased. The signals of both groups increased on D13- and subsequently increased on D17-.

Figure 5c shows that the signal intensities of the abdomen first increased and eventually decreased (D17-) after NP removal. As indicated in Fig. 6, after ZGOC and ZGOC–NH_2 exposure, NPs mainly accumulated in the guts, which indicated that the gastrointestinal tract was one of the possible excretion routes. The increased signal intensities in the gills might be induced by adhesion of the excreted particles. In other reports, urination via the kidneys (Singh et al. 2006) and defecation via the biliary duct (Renaud et al. 1989) are regarded as the primary routes of elimination. Of

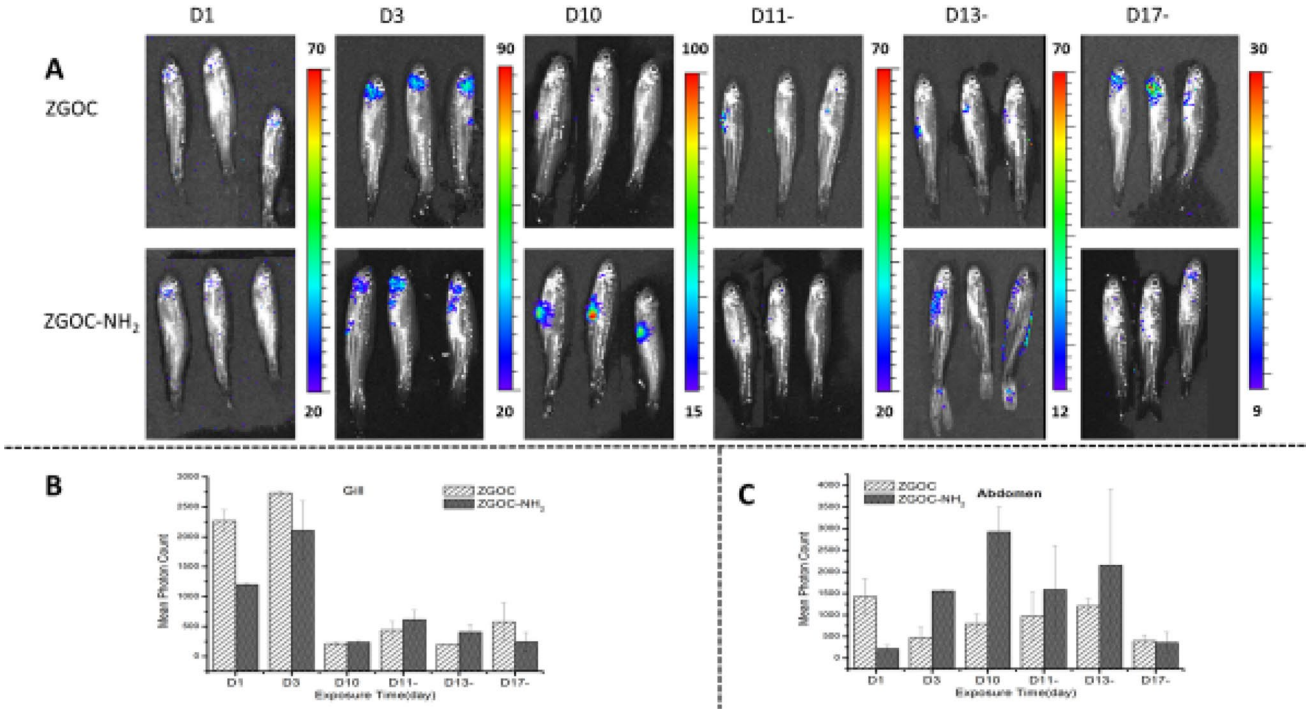

Fig. 5 Detection sensitivity for ZGOC/ZGOC–NH_2 in vivo. **a** In vivo luminescence images of zebrafish after 120 s of irradiation with a white-light LED lamp. The scale of counts ranges from 20 to 70, 20 to 90, 15 to 100, 20 to 70, 12 to 70, and 9 to 30. **b** and **c** The mean photon count of different parts of zebrafish in the two groups. Error bars represent the SD in a triplicate experimental set. "*" indicates significant differences between the two groups ($p < 0.05$)

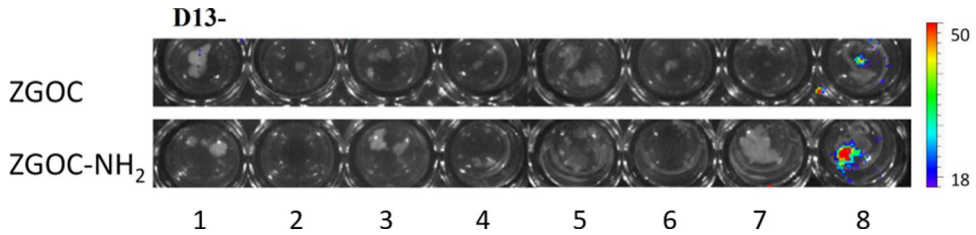

Fig. 6 In vitro luminescence images of zebrafish organs. Luminescence images of isolated organs after removal from exposure to ZGOC/ZGOC–NH_2 on the third day. (*1*) Brain (*2*) heart (*3*) liver (*4*) spleen (*5*) gill (*6*) kidney (*7*) gonads, and (*8*) gut. The scale ranges from 18 to 50

course, many other routes of elimination exist, such as sputum, perspiration, mammary lacteal glands, spermatic fluids and exhaled breath.

The main viscera of the zebrafish were dissected, and the signal intensities revealed the biodistribution of NPs. Figure 6 shows the results for the two experimental groups on D13-. NPs were found in the gut in both groups, whereas NPs in other organs were not clearly observed from the figure.

In this work, we utilized NIR persistent luminescence imaging to reveal the NP distribution in zebrafish. Compared with other imaging techniques (Bisesi et al. 2014; Li et al. 2014), the persistent luminescence imaging technique achieved long-time, high-sensitivity and in vivo detection of NPs.

Continuous exposure influences the uptake and biodistribution of NPs in vivo in adult zebrafish. Both the ZGOC- and ZGOC–NH_2-treated groups showed particle accumulation in the abdomen, especially in the intestines. The particle contents were higher in the ZGOC–NH_2-treated group than in the ZGOC-treated group, and continuous exposure caused damage to the gills and intestines. After a period of exposure, both the ZGOC and ZGOC–NH_2 particles could be excreted. The metabolism and excretion of NPs and the quantification and monitoring of NP behavior in biological systems should be examined in further studies.

Acknowledgements Thanks for financial support from the Bureau of International Cooperation, the Chinese Academy of Sciences (132C35KYSB20160021), The National Natural Science Foundation of China (21507129, 61705228), The Natural Science Foundation of Fujian Province, China (2018J05028).

References

Bergin IL, Witzmann FA (2013) Nanoparticle toxicity by the gastrointestinal route: evidence and knowledge gaps. Int J Biomed Nanosci Nanotechnol. doi: https://doi.org/10.1504/IJBNN.2013.054515

Bisesi JH, Merten J et al (2014) Tracking and quantification of single-walled carbon nanotubes in fish using near infrared fluorescence. Environ Sci Technol 48(3):1973–1983

Borm P, Klaessig FC, Landry TD et al (2006) Research strategies for safety evaluation of nanomaterials, part V: role of dissolution in biological fate and effects of nanoscale particles. Toxicol Sci 90(1):23–32

Chermont QL, Chaneac C, Seguin J et al (2007) Nanoprobes with near-infrared persistent luminescence for *in vivo* imaging. Proc Natl Acad Sci USA 104(22):9266–9271

Deng X, Jia G, Wang H et al (2007) Translocation and fate of multi-walled carbon nanotubes *in vivo*. Carbon 45:1419–1424

Evans DH, Piermarini PM, Choe KP (2005) The multifunctional fish gill: dominant site of gas exchange, osmoregulation, acid–base regulation, and excretion of nitrogenous waste. Physiol Rev 85:97–177

Furman O, Usenko S, Lau BLT (2013) Relative importance of the humic and fulvic fractions of natural organic matter in the aggregation and deposition of silver nanoparticles. Environ Sci Technol 43:1349–1356

Leguen I, Prunet P (2004) Effect of hypotonic shock on cultured pavement cells from freshwater or seawater rainbow trout gills. Comp Biochem Physiol A 137:259–269

Li JL, Shi JP, Shen JS et al (2014) Specific recognition of breast cancer cells in vitro using near infrared-emitting long-persistence luminescent $Zn_3Ga_2Ge_2O_{10}:Cr^{3+}$ nanoprobes. Nano–Micro Lett 7(2):138–145

Love DR, Pichler FB, Dodd A et al (2004) Technology for high-throughput screens: the present and future using zebrafish. Curr Opin Biotechnol 15:564

Mahmoudi M, Stroeve P, Milani AS et al (2010) Superparamagnetic iron oxide nanoparticles for biomedical applications. Nova Science Publishers, Inc. ISBN 978-1-61668-964-3

Maldiney T, Bessière A, Seguin J et al (2014) The *in vivo* activation of persistent nanophosphors optical imaging of vascularization, tumors and grafted cells. Nat Mater 13(4):418–426

Moller P, Jacobsen NR, Folkmann JK et al (2010) Role of oxidative damage in toxicity of particulates. Free Radic Res 44(1):1–46

Nel A, Xia T, Madler L et al (2006) Toxic potential of materials at the nanolevel. Science 311:622–627

Rallo R, France B, Liu R et al (2011) Self-organizing map analysis of toxicity-related cell signaling pathways for metal and metal oxide nanoparticles. Environ Sci Technol 45(4):1695–1702

Renaud G, Hamilton RL, Havel RJ (1989) Hepatic metabolism of colloidal gold-low-density lipoprotein complexes in the rat: evidence for bulk excretion of lysosomal contents into bile. Hepatology 9:380–392

Saxena RK, Williams W, Mcgee JK et al (2007) Enhanced in vitro and *in vivo* toxicity of poly-dispersed acid-functionalized single-wall carbon nanotubes. Nanotoxicology 1:291–300

Shi JP, Sun X, Li JL et al (2015) Multifunctional near infrared-emitting long-persistence luminescent nanoprobes for drug delivery and targeted tumor imaging. Biomaterials 37:260–270

Singh R, Pantarotto D, Lacerda L et al (2006) Tissue biodistribution and blood clearance rates of intravenously administered carbon nanotube radiotracers. Proc Natl Acad Sci USA 103:3357–3362

Stern HM, Zon LI (2003) Cancer genetics and drug discovery in the zebrafish. Nat Rev Cancer 3:533

Sun X, Shi JP, Zheng SH et al (2018) Visualization of inflammation in a mouse model based on near-infrared persistent luminescence nanoparticles. J Lumin 204:520–527

Wiesner MR et al (2006) Assessing the risks of manufactured nanomaterials. Environ Sci Technol 40(14):4336–4345

Yang RSH, Chang LW, Wu JP et al (2007) Persistent tissue kinetics and redistribution of nanoparticles, quantum dot 705, in mice: ICP-MS quantitative assessment. Environ Health Perspect 115:1339–1343

Zhu X, Wang J, Zhang X, Chang Y, Chen Y (2010) Trophic transfer of TiO_2 nanoparticles from daphnia to zebrafish in a simplified freshwater food chain. Chemosphere 79(9):928–933

Zou R, Gong SM et al (2017a) Magnetic-NIR persistent luminescent dual-modal ZGOCS@MSNs@Gd_2O_3 core–shell nanoprobes for in vivo imaging. Chem Mater 29(9):3938–3946

Zou R, Huang JJ et al (2017b) Silica shell-assisted synthetic route for mono-disperse persistent nanophosphors with enhanced in vivo recharged near-infrared persistent luminescence. Nano Res 10(6):2070–2082